Impact of the base doping concentration on the transport mechanisms in n-type a-SiGe:H/p-type c-Silicon Heterojunctions

P. Rosales-Quintero, M. Moreno-Moreno, A. Torres-Jacome, F.J. De la Hidalga Wade,
J. Molina-Reyes, W. Calleja-Arriaga, and C. Zuñiga-Islas
National Institute for Astrophysics, Optics and Electronics,
Electronics Department P.O.B. 51 & 216, Z.P 72000, Puebla, México,
Tel: (+52) 222-266-3100 ext 1411; Fax: (+52) 222-247-2742.
e-mail: prosales@inaoep.mx

The charge transport mechanisms occurring in n-type a-SiGe:H on p-type c-Si heterojunctions were determined by analyzing the temperature dependence of the current-voltage characteristics in structures with four different peak base doping concentrations ($N_B = 1 \times 10^{15}$, 7×10^{16}, 7×10^{17} and 5×10^{18} cm^{-3}). From the experimental results, we observed that at low forward bias (V< 0.45V) the current is determined by electron diffusion from the n-type amorphous film to the p-type c-Si for the heterojunction with $N_B = 1 \times 10^{15}$ cm^{-3}, whereas the Multi-Tunneling Capture Emission (MTCE) was identified as the main transport mechanism for the other base doping concentrations. On the other hand, at high forward bias (V> 0.45V), the space charge limited current effect became the dominant transport mechanism for all the measured devices. Under reverse bias the transport mechanisms depends on the peak base doping, going from carrier generation inside the space charge region for the lowest doping, to hopping and thermionic field emission as the base doping concentration is increased.

Keywords: Amorphous semiconductors; heterojunction diodes; transport mechanisms; base doping concentration.

Heterouniones de a-SiGe:H tipo-n sobre silicio cristalino tipo-p con cuatro diferentes concentraciones pico en la base (1×10^{15}, 7×10^{16}, 7×10^{17} y 5×10^{18} cm^{-3}) fueron fabricadas y caracterizadas. Los mecanismos de transporte se determinaron por medio de sus curvas características de corriente vs voltaje en función de la temperatura. El análisis de los resultados muestra que a bajos voltajes de polarización directa (V< 0.45V) en la heterounión con la menor concentración pico la corriente es determinada por la difusión de electrones del a-SiGe:H tipo-n hacia el silicio cristalino tipo-p. Mientras que el multituneleo captura-emisión (MTCE) es el principal mecanismo de transporte en las otras heterouniones. A altos voltajes de polarización directa (V> 0.45V) el efecto de corriente limitada por carga espacial (SCLC) es el mecanismo de transporte dominante en todos los dispositivos caracterizados. El incremento en la concentración de dopantes en la base, además, causa un aumento en la corriente inversa.

Descriptores: Semiconductores amorfos; heterouniones; mecanismos de transporte; concentración de dopantes en la base.

PACS: 85.30.Kk; 73.40.Lq; 73.50.Gr

1. Introduction

Since the optical band gap (Eg) of the a-SiGe:H films can be tailored from 1.7 eV to 1 eV by varying the germanium molar fraction, these films have been widely used in several devices such as solar cells, photodetectors, bolometers, and TFTs [1-4]. Nevertheless, new and novel applications for this heterojunction require a deep understanding of the physical properties and transport mechanisms governing its electrical behavior. Up to now, the current transport mechanisms involved in any kind of amorphous/crystalline heterojunction have not been fully addressed. Get in contrast several mechanisms have been proposed to be responsible for $J - V$ characteristics in a-Si:H/crystalline heterojunctions [5-9]. Recently, in Ref. 10 it has been shown that one source for the disagreement among the proposed mechanisms can be attributed to the different thicknesses for the amorphous layers used in the fabrication of those heterojunctions. It is also believed that the doping concentration of the crystalline silicon base can present a strong influence on those transport mechanisms. Therefore, a study was performed in order to assess the impact of the base doping on the transport properties. First, the fabrication process for the heterojunction diodes is described in Sec. 2. Next, in the Sec. 3, a discussion of the current-voltage characteristics of the junctions at different temperatures is presented. Finally, the conclusions of this work are presented in Sec. 4.

2. Experiment

The initial material was a boron doped p-type crystalline silicon wafer with an average concentration of 1×10^{15} cm^{-3}. A boron implantation was performed on the back surface of the wafer to improve the back contact, whereas 500 nm of silicon oxide was thermally grown on the top surface. Windows were

TABLE I. Doses and peak doping concentrations on the wafers

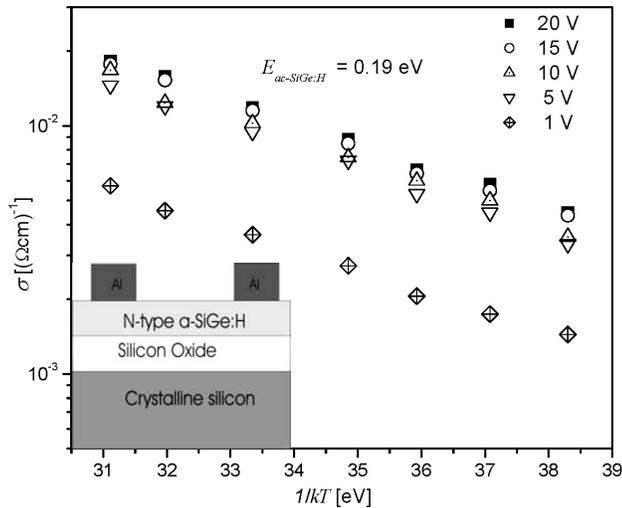| Wafer	DOSE [cm^{-2}]	Peak concentration [cm^{-3}]
W1	No implantation	1×10^{15}
W2	1×10^{13}	7×10^{16}
W3	5×10^{13}	7×10^{17}
W4	5×10^{14}	5×10^{18}

FIGURE 1. Thermal dependence of σ at different voltages. Inside cross section view of the aluminium electrodes stripes structure.

opened on the silicon oxide using photolithography in order to define the area of the heterojunctions; thus a subsequent 120 nm thermal oxide was grown on such windows and a 40 KeV boron implantation was conducted for different doses on 3 wafers. The different boron doses and the obtained peak surface concentrations are shown in Table I. After etching 120 nm of thermal oxide on the windows, the silicon surface was cleaned and passivated by HF dip, a 200 nm film of n-type a-SiGe:H was deposited on the crystalline silicon surface. Finally, aluminum was e-beam evaporated on the top and back surfaces of the wafers. The a-SiGe:H films were deposited at 300°C using a Low Frequency (110 kHz) PECVD system. The precursor gases were SiH_4 and GeH_4 with hydrogen dilution. The gas flow ratio R=[GeH$_4$]/[GeH4+SiH$_4$] was set to 1/10, and the n-type doping was achieved by adding phosphine to the reactive gases using a gas flow ratio of R=[PH$_3$]/[SiH$_4$+GeH$_4$+ PH$_3$] = 1/6. In order to obtain the DC conductivity at different temperatures $\sigma(T)$ of the a-SiGe:H layers, stripes of aluminum were used as electrodes with a 1-2 mm inter-electrode separation. The Al electrodes were deposited by e-beam evaporation on the silicon oxide substrates after the film deposition (the cross section view of the structure is shown at the onset of Fig. 1). The measurements of $\sigma(T)$ were conducted under dark conditions, and the results are presented in Fig. 1. According to [11], this dependence can be expressed as:

$$\sigma(T) = \sigma_0 \exp\left[-\frac{E_{ac\text{-SiGe:H}}}{kT}\right],\qquad(1)$$

where σ_0 is a pre-factor, $E_{ac\_\text{SiGe:H}}$ is the activation energy, k is the Bolztmann's constant, and T is the absolute temperature. As can be seen in Fig. 1, the value of $E_{ac\_\text{SiGe:H}}$=0.19 eV is consistent with the value estimated from the gas flow ratio of [PH$_3$]/[SiH$_4$+PH$_3$] [11]. We calculated the effective donor doping concentration in the amorphous film ($N_{\text{Damorphous}}$) using the value of $E_{ac\_\text{SiGe:H}}$ and the following relationship [12]:

$$N_{\text{Damorphous}} = N_C \exp\left[-\frac{E_{ac\text{-SiGe:H}}}{kT}\right],\qquad(2)$$

where N_C=1×10^{20} cm^{-3} is the typical effective density of states in the conduction band [12]. Then, at 300 K, the calculated effective doping concentration was

$$N_{\text{Damorphous}} \approx 5 \times 10^{16} \text{cm}^{-3}.$$

3. Results and discussion

3.1. Current - voltage characteristics

Figure 2 shows the *J-V* behavior of the four fabricated heterojunctions, which were measured using an HP4156B Semiconductor Parameter Analyzer, at temperatures varying between 295 and 381 K. In the same figure, it can be seen that the forward current density shows two different regions for all the heterojunctions. For V< 0.45V, the current density increases exponentially as a function of the applied voltage, and the J-V behavior can be described by [11]:

$$J = J_0\left[\exp\left[AV\right] - 1\right],\qquad(3)$$

where A is a coefficient defined as:

$$A = \frac{q}{\eta kT}\qquad(4)$$

η is the ideality factor and J_0 is the saturation current density:

$$J_0\alpha \exp\left[-\frac{E_{ac}}{kT}\right]\qquad(5)$$

In this equation E_{ac} is the activation energy measured with respect to the top of the valence band. As can be seen from (4) and (5) these parameters depend on both, the transport mechanisms, characterized by η and temperature. Therefore, the values of the ideality factor can give some insight into the current transport mechanisms. For instance, if the forward-bias transport is limited by diffusion, then $\eta = 1$. On the other hand, if the transport is limited by recombination at the space charge region (SCR), then $\eta = 2$. If tunneling controls the current, A will not depend on temperature.

On the other hand, for all measured diodes it was noticed that when the applied forward voltage was increased above 0.45 V, the $J - V$ characteristics deviated from the ideal behavior. If all the curves in Fig. 2 are plotted in log-log scale for V> 0.45V, it can be seen that the $J-V$ characteristics will show either a linear or a power law; therefore, they present a space charge limited characteristic (SCLC), and the relationship can be described as [13,14]:

$$J = KV^M\qquad(6)$$

Here K is a function of the film thickness and trap distribution, whereas M is a parameter that depends on the density of states in the amorphous layer.
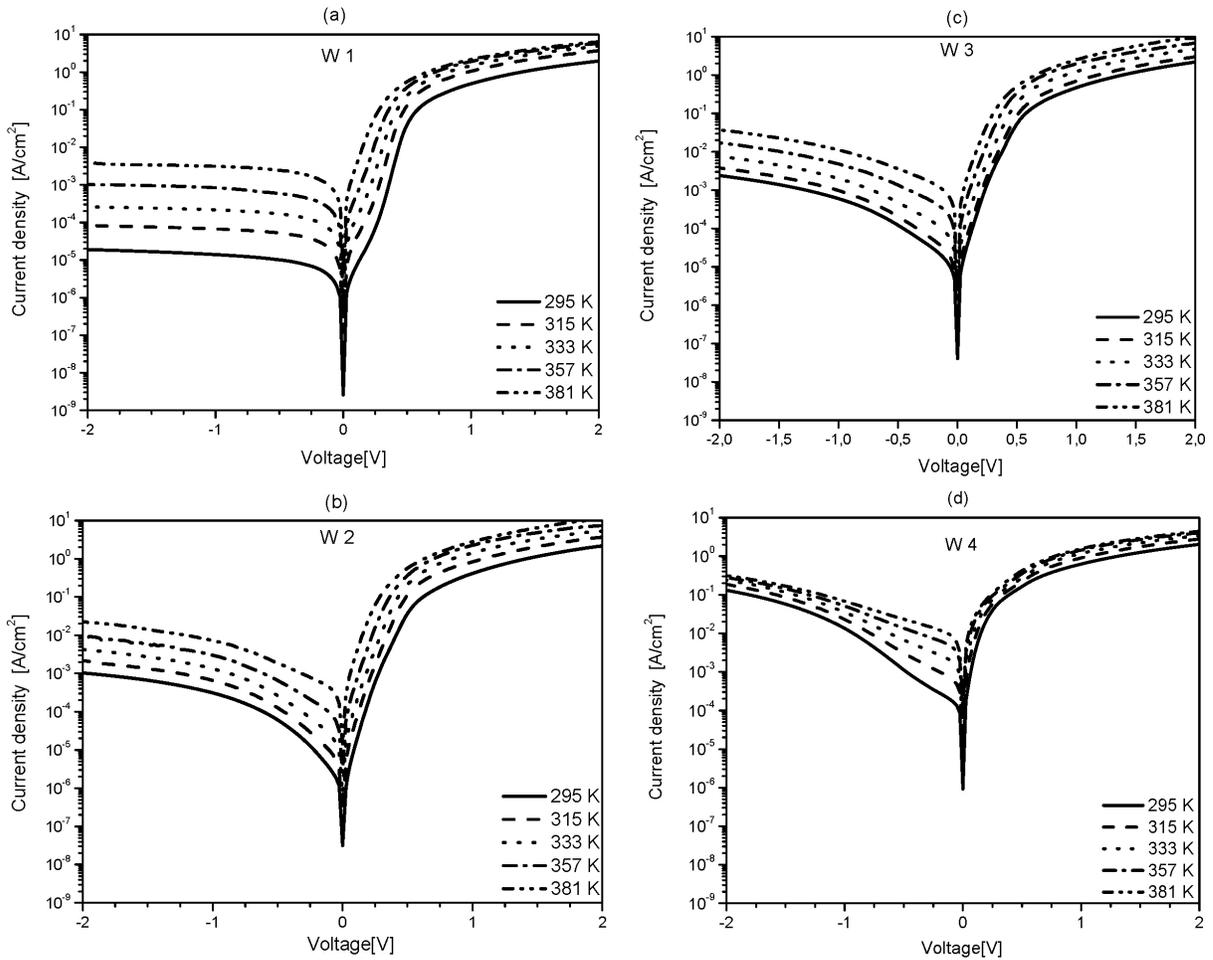
FIGURE 2. $J - V$ curves of n a-SiGe:H/p-crystalline silicon heterojunction diodes at different temperatures.
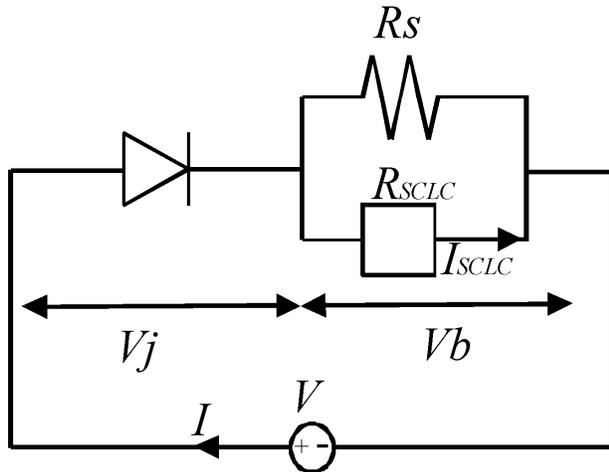

FIGURE 3. Electrical equivalent circuit for the amorphous/c-Si heterojunction.

The traditional method used to extract the values of η and E_{ac} from the $J - V$ characteristics is based on the plot of $\log(J)$ vs V. However, this approach usually does not take into account the possible series resistance that is present in a real diode or a heterojunction. As a consequence, there is certain degree of uncertainty associated with this method, and the accuracy of the values obtained for η depends on the value of that series resistance. In order to overcome this problem, Marsal *et al.* [15] have proposed a physically-based electrical model for the amorphous/crystalline heterojunction. This model separates the rectifying behavior (V_j) from the bulk effects (V_b). Then, in this work the parameters A, Jo, K, M and the series resistance (Rs) were determined by fitting the $J - V$ characteristic as a function of temperature using Marsal's circuit equivalent shown in Fig. 3. Figure 4 shows the experimental and simulated $I - V$ characteristics obtained at 295 K. As can be seen, a good agreement between the experimental and simulated data is obtained when the model proposed by Marsal [14] is used.

Figures 5 (a) and (b) show the Arrhenius plots of A and J_0 for all the samples. From Fig. 5(a), we obtained η=1.10 for wafer W1. When J_0 is plotted as a function of the inverse of temperature, a linear behavior is observed as shown in Fig. 5(b), and $E_{ac} = 1.05$ eV was calculated. As can be

TABLE II. Transport mechanism reported in the literature for some amorphous semiconductors/c-Si heterojunctions operating under forward bias.

Ref.	AMORPHOUS layer	THICKNESS [NM]	Doping concentration [cm^{-3}]		Transport mechanism
			a-Si	c-Si	
Magafas [16]	a-SiC:H	1000	intrinsic	1×10^{15}	SCR-G
Matsuura [5]	a-Si:H	1200	intrinsic	1×10^{16}	MTCE
Marsal [7]	a-Si:H	500	7×10^{15}	1×10^{16}	SCR-G
Marsal [17]	a-SiC:H	200	2×10^{17}	1×10^{16}	SCR-G
Marsal [6]	a-SiC:H	200	2×10^{17}	1×10^{18}	MTCE
Marsal [6]	a-SiC:H	200	2×10^{17}	1×10^{20}	MTCE
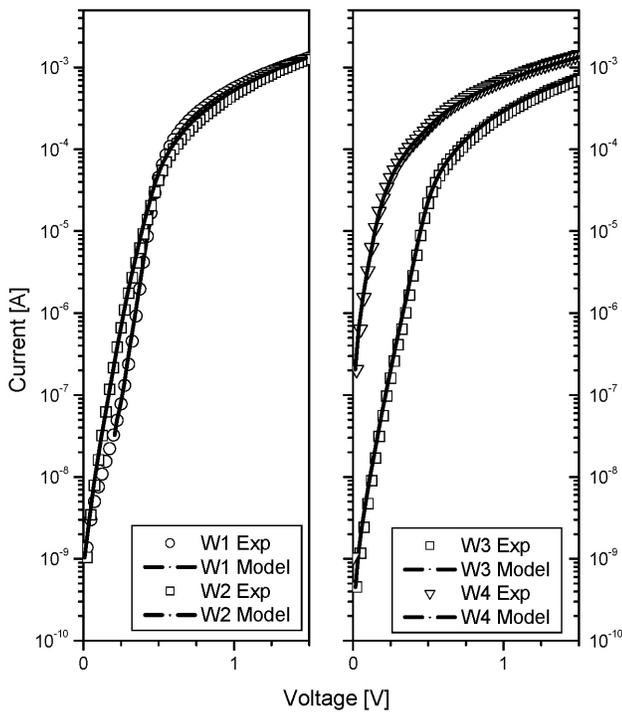
FIGURE 4. The experimental and simulated current-voltage characteristics at 295 K.

FIGURE 5. Arrhenius plots of A and J_0.

seen, this value is close to the crystalline silicon band gap (1.12 eV), which together with the value obtained for η, leads to the conclusion that the electron diffusion in the crystalline region determines the transport mechanism in W1. Regarding to the W2, W3 and W4 wafers, we observed that A did not depend on temperature, and activation energies of 0.6, 0.55 and 0.50 eV, respectively, were calculated. This kind of behavior is typical of the tunneling mechanism for conduction, which is independent on temperature. Among the several tunneling mechanisms, the conduction seems to follow the MTCE model, which is widely believed to be one of the dominant mechanisms in a-Si:H/c-Si heterojunctions [5]. This is reasonably explained by both, the increased probability of multi-step tunneling, resulting from the continually distributed localized states within the band gap of a-SiGe:H,
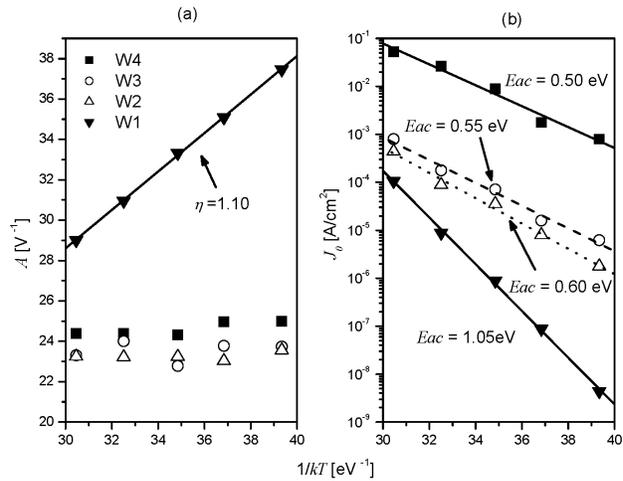
and the linear behavior of J_0 vs $1/kT$ in Fig. 5(b). In the MTCE model, J_0 is described by [5]:

$$J_0 = B_{SCLC}\left[\sigma_p v_{th} N_V \exp\left[-\frac{E_T - E_V}{kT}\right]\right.$$

$$\left. + \sigma_n v_{th} N_C \exp\left[-\frac{E_C - E_F}{kT}\right]\right], \tag{7}$$

where B_{SCLC} is a voltage and temperature-independent coefficient, σ is the capture cross section, ν_{th} is the thermal velocity, and the subscripts n and p stand for electrons and holes, respectively. N_C and N_V are the effective density of states in conduction and valence bands, and E_T and E_F are the trap and Fermi level, respectively.

Based on these results, the deep defects determine the dominant transport mechanism in all heterojunctions, and an increase in the mid-gap recombination is observed. We can assume that η goes to 2. Nevertheless, when the base doping concentration is higher than 1×10^{15} cm^{-3}, the probability of multi-step tunneling increases, and this leads to a change in the dominant transport mechanism. As it is shown in Fig. 5(b), J_0 is dominated by the first term in the right side of (7), and a hole emission rate higher than the electron cap-
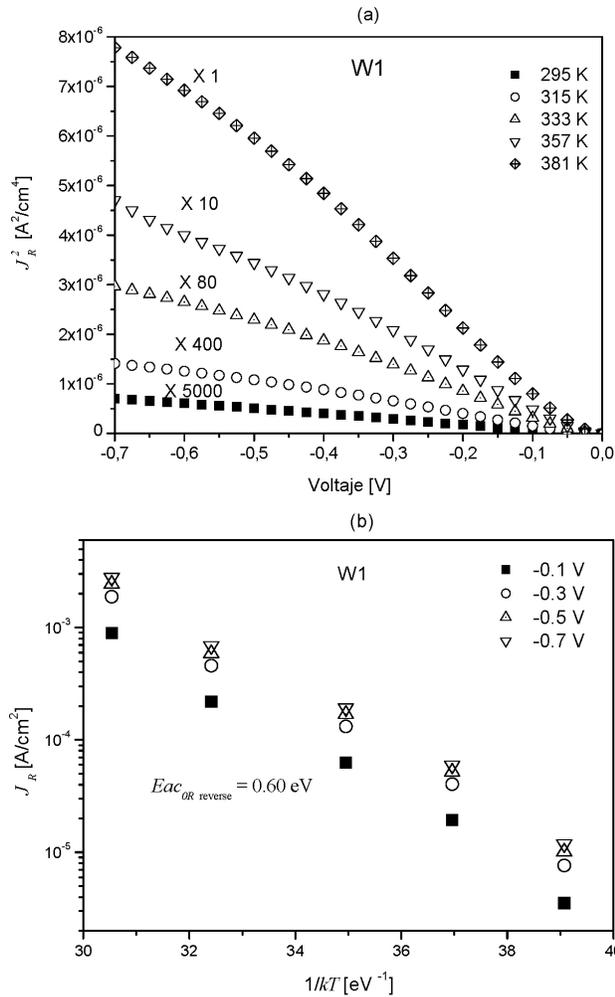
FIGURE 6. (a) The values of J^2 are amplified by a factor, which is noted in the figure. (b) J_0 at different reverse bias voltages obtained from W1 as a function of temperature.

FIGURE 7. (a) and (b). Current density at Vr=-0.5, -1 and -1.5 V as a function of the temperature for W2 and W3, respectively.

ture rate seems to be responsible for this result. Our conclusions are supported by the transport mechanisms identified and reported [5,6,16,17] for different amorphous/crystalline heterojunctions, which are shown in Table II.

3.2. Reverse dark J-V characteristics

In previous works [5-7], several authors found that the reverse current density J followed the relationship $J^2 \alpha V$. As shown in Fig. 6(a), J^2 is a linear function of the applied reverse voltage from 0 to 0.7 V for sample W1. From this behavior, we can say that the reverse J is dominated by the carrier generation inside the space charge region. Also, Fig. 6(b) shows the current density characteristics at different temperatures for Vr = -0.1, - 0.2 and -0.5 V, resulting in an "*Eac reverse*" of 0.60 eV. This value is close to half of the silicon band gap, showing that the crystalline silicon determines the electrical behavior. However, the heterojunctions fabricated on the W2, W3, and W4 samples do not follow this relationship. Thus, the J generated in the depletion region does not dominate the reverse current. As it is well known, all amor-
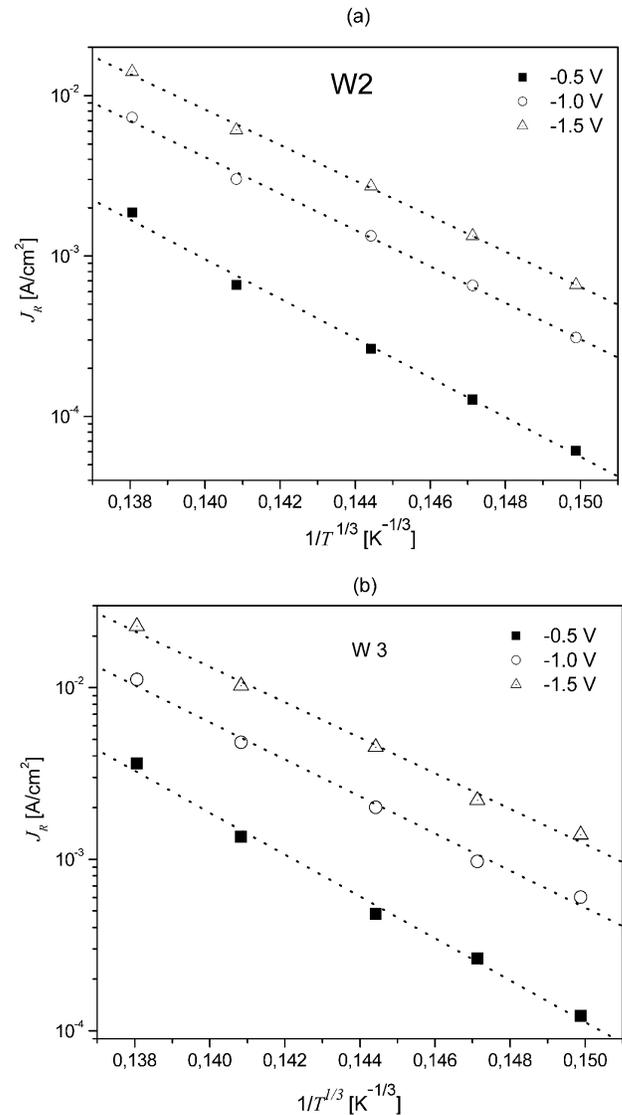
phous semiconductors present a continuous trap distribution along their band gap, and the way in which this trap distribution can contribute to the reverse current is by the hopping of thermally generated electrons. The dependence on the temperature of the reverse current density is described as [16]:

$$J = A_H \exp\left[-\frac{B}{T^{\frac{1}{N}}}\right], \qquad (8)$$

where A_H is a weakly temperature dependent quantity, B is a constant and N is a parameter whose value can be 4 or 3. If $N = 4$ Eq. (9) will corresponds to the Mott's $T^{-1/4}$ law, applicable for the transport in the three dimensional case; for the two dimensional case, we will have $J\alpha T^{-1/3}$. For the W2 and W3 samples, we found that the reverse current is proportional to $T^{-1/3}$ at -0.5, -1.0 and -1.5 V, showing similar slopes (Fig. 7). These results suggest that the reverse current is influenced by the thermally activated electron contribution coming from the deep traps.
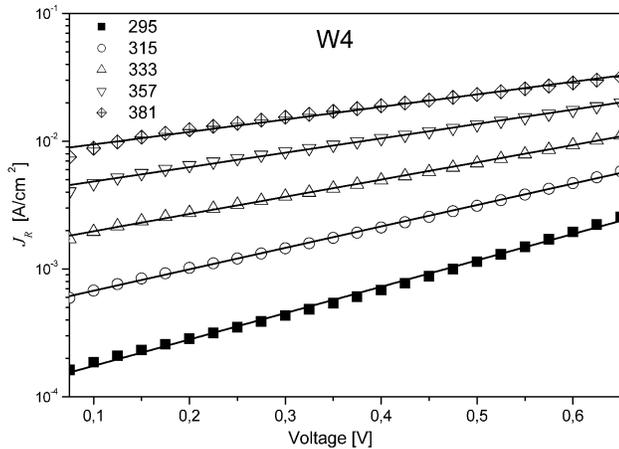
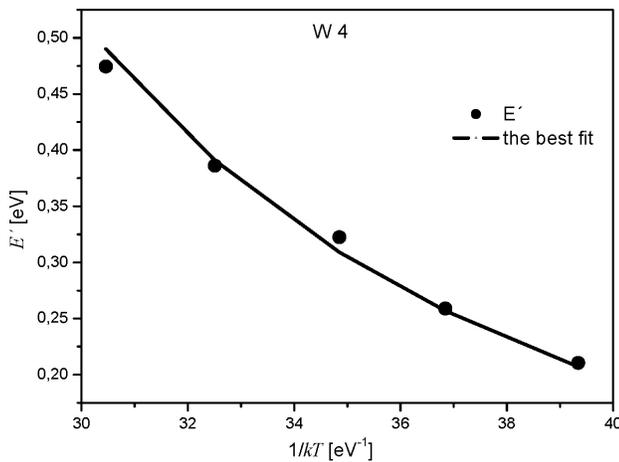FIGURE 8. Reverse current density as a function of the temperature for W4.

FIGURE 9. E' calculated at reverse bias voltage as a function of the temperature for W4.

Finally, Fig. 8 shows that the heterojunctions fabricated on the W4 sample follow none of the previous transport mechanisms. In this case, the current density can be due to thermionic field emission (TFE), which occurs in either metal-semiconductor junctions or highly doped junctions. The TFE can be described by [18]:

$$J_R = J_{0R} \exp\left[\frac{qV_R}{E'}\right], \qquad (9)$$

where J_{0R} is the reverse saturation current density, V_R is the applied voltage, and the energy E' is given by [18]:

$$E' = E_{00} \coth\left[\frac{E_{00}}{kT}\right] \left[\left[\frac{E_{00}}{kT}\right] - \tanh\left[\frac{E_{00}}{kT}\right]\right]^{-1} \qquad (10)$$

The parameter E_{00} is a property of the bulk [18]:

$$E_{00} = \frac{q\hbar}{2}\sqrt{\frac{N_B}{\varepsilon_B m*}}, \qquad (11)$$

where $\hbar$ the reduced Planck constant, N_B is the bulk doping concentration, ε_B is the permittivity of the bulk, and $m*$ is the carrier effective mass.

Figure 9 shows the values of E' obtained from the experimental curves shown in Fig. 8; the best fit for E' was obtained when a value of 21.1 meV was used for E_{00}. The value of $m^*=0.38m_0$ was estimated by using 21.1 meV for E_{00} in Eq. (10), which agrees with that value reported in Ref. 19 for the hole effective mass for conductivity calculations in crystalline silicon.

4. Conclusions

In this work, we have investigated the effects of the base doping concentration on the transport mechanisms for n-type a-SiGe:H on p-type c-Si heterojunctions. The current-voltage measurements indicated that the current transport mechanisms for forward and reverse bias are strongly dependent on the base doping concentration. For the $0< V <0.45$ V voltage range, the electron diffusion from the n-type a-SiGe:H to the crystalline part of the structure determines the transport mechanism for the heterojunctions with the lowest base doping concentration. The Multi-Tunneling Capture Emission is the dominant mechanism for the diodes fabricated with base doping concentrations above of 1×10^{15} cm^{-3}. On the other hand, for voltages above 0.45 V, the series resistance affects strongly the transport, and the space charge limited effect becomes the main transport mechanism for all the measured devices. Under reverse bias conditions, the transport mechanism is dominated by the carrier generation inside the space charge region for the wafer with a base doping concentration of 1×10^{15} cm^{-3}. Hopping through the localized states into the gap is the main transport mechanism for the wafers with a base doping concentrations of 7×10^{16} and 7×10^{17} cm^{-3}, whereas for a base doping concentration of 5×10^{18} cm^{-3}, TFE is the main transport mechanism.

1. W. Luft and Y. Simon Tsuo, *Hydrogenated Amorphous Silicon Alloy Deposition Process* (Marcel Dekker, Inc., 1993). pp. 27.

2. A. Kosarev, M. Moreno, A. Torres, S. Rumyantsev, and I. Cosme, *Thin Solid Films* **518** (2009) 3310.

3. M.L. García Cruz, A. Torres, A. Kosarev, and R. Ambrosio, *Journal of Non-Crystalline Solids* **329** (2003) 179.

4. M.A. Jiménéz Domínguez, (Master Thesis in Spanish, INAOE, Puebla, Mexico, 2008).

5. H. Matsuura, *IEEE-TED* **36** (1989) 2908.

6. L.F. Marsal, J. Pallarés, X. Correig, J. Calderer, and R. Alcubilla, *Semiconductor Sci. Technol.* (1998) 1148.

7. L.F. Marsal, J. Pallarés, X. Correig, J. Calderer, and R. Alcubilla, *J. Appl. Phys.* **70** (1996) 8493.

8. Ping Li, Q. Yong, C. Andre, and T. Salama, *IEEE-TED* **41** (1994) 932.

9. Z.R. Tang T. Kamins, C. Andre, and T. Salama, *IEEE-TED* **14** (1993) 348.

10. P. Rosales-Quintero *et al.*, *J. Appl. Phys.* **97** (2005) 97.

11. Jerzy Kanicki, *Amorphous and Microcrystalline Semiconductor Devices* Vol. II (Artech House, Inc., chapter 11, 1992). pp 542.

12. D.M. Garner and G.A.J. Amaratunga, *IEEE-ED* **43** (1996) 1890.

13. C. Zúñiga-I *et al.*, *Phys. Status Solidi C* **7** (2010) 808.

14. L.F. Marsal, J. Pallarés, X. Correig, J. Calderer, and R. Alcubilla, *Semiconductor Sci. Technol.* (1996) 1209.

15. A. Rose, *Phys. Rev.* **97** (1955) 1538.

16. L. Magafas, N. Georgoulas, and A. Thanailakis, *Semiconductor Sci. Technol.* (1992) 1363.

17. L.F. Marsal *et al.*, *J. Appl. Phys.* **85** (1999) 1216.

18. R.J. Nemanich and M.J. Thompson, *in: B.L. Sharma, Editor. Metal Semiconductor Schottky Barrier Junction and Their Applications* (Plentum Press, Inc., Chapter 9, 1984). pp. 52.

19. B. Van Zeghbroeck (2007). Principles of Semiconductor Devices. Chapter. 2. Sec. .2.6.4.2 appendix 3. Available: http://ecee.colorado.edu/∼bart/book/